Catalysis Today 183 (2012) 26–33

Contents lists available at ScienceDirect

Catalysis Today

journal homepage: www.elsevier.com/locate/cattod

Water assisted synthesis of double-walled carbon nanotubes with a narrow diameter distribution from methane over a Co–Mo/MgO catalyst

Gaowei Wang[a], Jiuling Chen[b], Ye Tian[a], Yi Jin[a], Yongdan Li[a,*]

[a] Tianjin Key Laboratory of Applied Catalysis Science and Technology and State Key Laboratory of Chemical Engineering (Tianjin University), School of Chemical Engineering, Tianjin University, Tianjin 300072, China
[b] Division of Chemical Engineering, School of Engineering, The University of Queensland, St Lucia QLD 4072, Australia

ARTICLE INFO

Article history:
Received 17 April 2011
Received in revised form 4 July 2011
Accepted 5 July 2011
Available online 3 August 2011

Keywords:
DWCNTs growth
Narrow diameter distribution
Water-assisted CVD
Co–Mo/MgO catalyst

ABSTRACT

Double-walled carbon nanotubes (DWCNTs) with a narrow diameter distribution have been synthesized with the assistance of water vapor in a fluidized-bed reactor from methane over a Co–Mo/MgO catalyst. The results reveal that an appropriate amount of water enhances the carbon yield and also changes the diameter distribution of the DWCNTs. An excess amount of water depresses the formation of carbon nanotubes due to the stabilization of the Co–molybdate phase. Water facilitates the formation of adjacent Co and CoO phases, and therefore methane activation and carbon nanotube formation. The formation of adjacent Co and CoO phases results in smaller Co nanoparticles. DWCNTs with narrow diameter distribution are produced with this method at a low cost.

1. Introduction

Since the publication of Iijima in 1991 [1], carbon nanotubes (CNTs) have been a category of the most actively investigated materials both in physics and chemistry sectors [2]. CNTs have potential applications in field emitters, super capacitors, chemical sensors, and selective membranes etc. [3–7]. Recently, the catalytic grown carbon nanofibers and CNTs are found superior to be used as the fuel of a direct carbon fuel cell, based on which, a highly efficient chemical energy conversion system can be composed [8–14]. It has been also convinced that CNTs with smaller diameters are better for all the above mentioned application purposes, even for using as the fuel of a fuel cell [15–17]. However, the large-scale production of CNTs is still a challenge.

Several methods have been investigated in the past few decades for the production of CNTs. These include high-pressure CO (HiPco) disproportionation [18], arc discharge-vaporization of graphite [19], laser ablation of carbon [20], and catalytic chemical vapor deposition (CVD) [21–25] etc. CVD is a low-cost technique and has the potential to be well controlled and scaled up. Therefore, this method has received enormous attention. In order to improve the efficiency of the CNT production, various ideas for enhancing the processes have been proposed. Water assisted CVD was proposed by Hata et al. [26] and has been taken as a milestone towards the high efficient production of pure single-walled (SW) CNTs and been called as the "super-growth" process [27]. Although the role of water is not yet fully understood, it is evident that the addition of a small and specific amount of water leads to the enhancement both in the growth height and nucleation density of the CNTs [28–30].

Double-walled (DW) CNTs, being the simplest example of multi-walled (MW) CNTs, have also attracted a considerable scientific interest. DWCNTs have a unique structure, which exhibits remarkable optical, mechanical and electronic properties. The structure provides an ideal model for the study of the interlayer physical and chemical interactions of CNTs, and facilitates the development of new applications if the external wall is functionalized [31]. DWCNTs have been synthesized successfully with the CVD method [32–37]. Ning et al. [38] prepared a lamella-like Fe/MgO catalyst by hydrothermal treatment and achieved a high yield of DWCNTs. Qi et al. [39] used iron disilicide ($FeSi_2$) as the catalyst and obtained a DWCNT sample with over 90% purity and a narrow diameter distribution in the range of 4–5 nm. Fluidized bed reactor was employed to facilitate a large-scale synthesis of DWCNTs [40]. However, the synthesis of DWCNTs with a narrow diameter distribution and high efficiency is still a challenge.

Bimetallic Co–Mo catalyst, after being widely used for decades due to its high activity in hydrodesulphurization [41,42], has attracted much attention because of its high selectivity for the growth of SWCNTs [43–45]. Methane has been chosen as the carbon source in this work because of its high stability at elevated temperature, which eliminates the self-pyrolysis leading to the generation of amorphous carbon and causing catalyst deactivation [22,23].

* Corresponding author. Tel.: +86 22 27405613; fax: +86 22 27405243.
E-mail address: ydli@tju.edu.cn (Y. Li).

0920-5861/$ – see front matter © 2011 Elsevier B.V. All rights reserved.
doi:10.1016/j.cattod.2011.07.004

MgO is an appropriate support because it can be easily removed by acid solution without damaging the structure of the CNTs [21,46]. In this work, we examine the effect of water during the synthesis of DWCNTs over a Co–Mo/MgO catalyst in a CH_4 and Ar mixed feed. To the best of our knowledge water vapor assisted CNT synthesis over Co–Mo catalysts has not been investigated. The role of water in the process is discussed.

2. Experimental

2.1. Catalyst preparation

Co–Mo/MgO (Co and Mo mole ratio 1:1) was prepared with a total metal loading of 10 wt.%. In the preparation, $Co(NO_3)_2$ aqueous solution (0.1 M) and $(NH_4)_6Mo_7O_{24}$ aqueous solution (0.05 M) were used. Stoichiometric amount of MgO powders was mixed with the aqueous solution of salts and stirred at 70 °C. After 8 h, the slurry was formed and the material was dried at 140 °C for 12 h in an oven. The dried product was then calcined at 450 °C for 5 h. Finally, the material was ground and sieved. The particles with a size between 200 and 250 mesh were used in the reaction.

2.2. DWCNT growth

The growth of DWCNTs was carried out at 850 °C in a quartz fluidized bed reactor with an inner diameter of 12 mm. 300 mg catalyst was loaded for each run. Before the reaction, the catalyst was reduced in situ at 550 °C for 1 h with a flow of H_2/Ar 1:1 in a total flow rate of 360 ml min^{-1} (STP). At the prescribed temperature the feed was switched to the reactant stream of CH_4/Ar 1:4 in volume. Water vapor was introduced into the reactor by controlling different amount of Ar bubling through a water saturator, and the total flow rate was kept at 360 ml min^{-1} (STP). The gaseous product was measured by an online Agilent 6890 GC equipped with a thermal conductivity detector (TCD). The reaction lasted for 45 min, after that, the reactor was cooled down to room temperature in Ar atmosphere. The carbon yields were calculated as:

$$\text{Carbon yield} = \frac{m_{\text{product}} - m_{\text{catalyst}}}{m_{\text{catalyst}}}$$

2.3. Characterization

X-ray diffraction (XRD) measurements were performed on a Rigaku D-max diffractometer using Cu kα radiation. The step-scans were taken over the range of 2Θ from 10 to 90 °C in step of 0.02 °C and the intensity data for each one was collected for 0.15 s.

Temperature-programmed reduction (TPR) experiments were performed in a "U" shaped reactor with an internal diameter of 4 mm in a ChemBET 3000 analysis system with a TCD. 10 vol.% H_2 in He was used as reduction gas with a total flow rate of 50 ml min^{-1} (STP). The heating rate was 10 °C min^{-1} and the catalyst amount was 10 mg for each experiment.

The morphologies and microstructures of the as-synthesized carbon materials were characterized by a FEI Tecnai G2 F20 high-resolution transmission microscope (HRTEM). The samples were prepared by sonication of the as synthesized product in ethanol and dropping of the suspension onto a Cu TEM grid with a carbon film. Raman spectra was recorded by a DXR Smart Raman Spectrometer of Thermo Fisher Scientific with Nd:YAG (532 nm) as excitation source. The carbon materials deposited on the catalysts were also characterized by thermogravimetry (TG) analysis. The weight loss of the carbon materials was observed in an atmosphere of air with a heating rate of 5 °C min^{-1} in a Perkin-Elmer Pyris 6 TGA. The flow rate of air was 30 ml min^{-1} (STP).

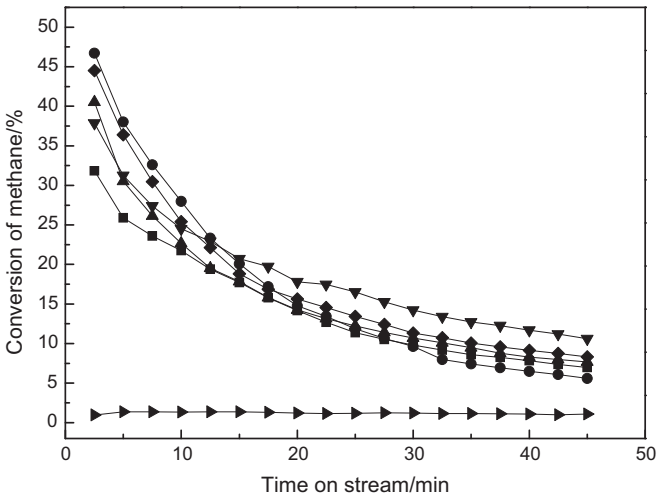

Fig. 1. The conversion of methane as a function of reaction time over Co–Mo/MgO catalyst under different content of water vapor: (■) 0 ppm, (●) 460 ppm, (▲) 930 ppm, (▼) 1400 ppm, (♦) 1970 ppm and (►) 4670 ppm.

3. Results and discussion

3.1. Catalyst activity

Fig. 1 shows the promoting effect of water in ppm level on the conversion of methane with the extension of time on the Co–Mo/MgO catalyst. Compared with that without the addition of water, the conversion of methane is enhanced, especially at the initial stage. However, too much water inhibits the decomposition reaction. When the concentration of water is 4670 ppm, the conversion of methane is close to zero. 47.3 wt.% carbon materials are produced on the catalyst without the assistance of water vapor, while the maximum carbon yield reaches 63.4 wt.% when the concentration of water is 460 ppm and no carbon is produced when the concentration of water is 4670 ppm. Therefore, the addition of water in the suitable concentration is advantageous to the growth of CNTs, which is consistent with the earlier reports with Fe/Al_2O_3 and Fe–Mo/MgO catalysts for the growth of SWCNTs [26,47].

3.2. Catalyst structure

In order to identify the structure of the catalyst, Co/MgO catalyst with a metal loading of 10 wt.% was also included for XRD

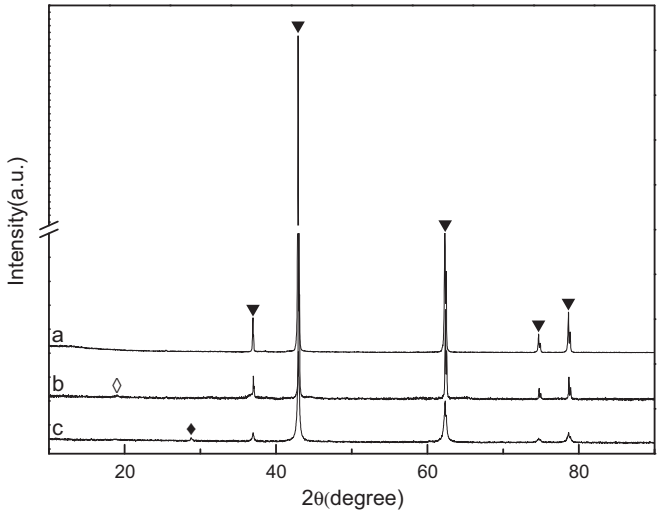

Fig. 2. XRD patterns of (a) MgO support, (b) Co/MgO catalyst and (c) Co–Mo/MgO catalyst; (▼) $Co_xMg_{1-x}O$, (♦) $MgMoO_4$ and (◊) Co_3O_4.

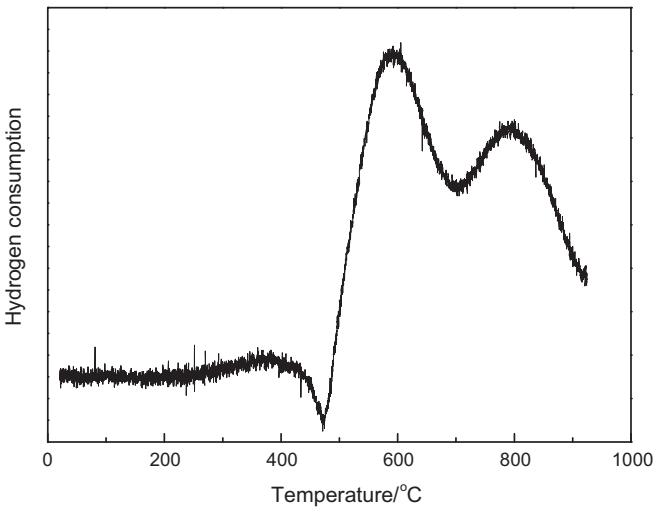

Fig. 3. H_2-TPR profile of Co–Mo/MgO catalyst.

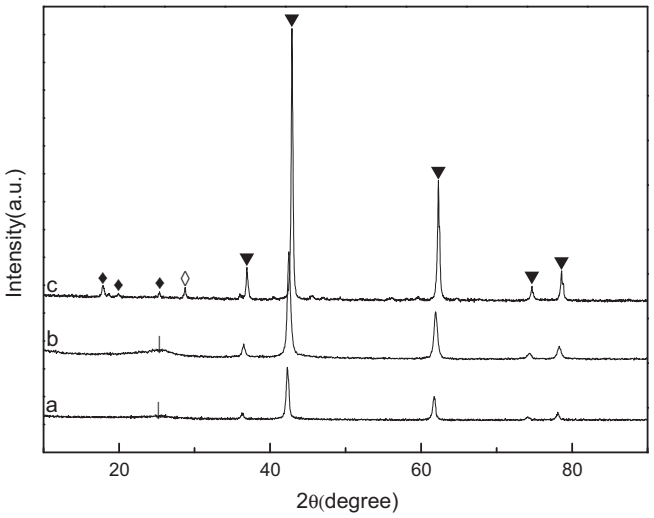

Fig. 4. XRD patterns of (a) Co–Mo/MgO catalyst after reaction without water vapor assistance, (b) Co–Mo/MgO catalyst after reaction with water vapor of 460 ppm and (c) Co–Mo/MgO catalyst after reaction with water vapor of 4670 ppm; (▼) $Co_xMg_{1-x}O$, (◊) $MgMoO_4$, (♦) $Co_2Mo_3O_8$ and (↓) CNT.

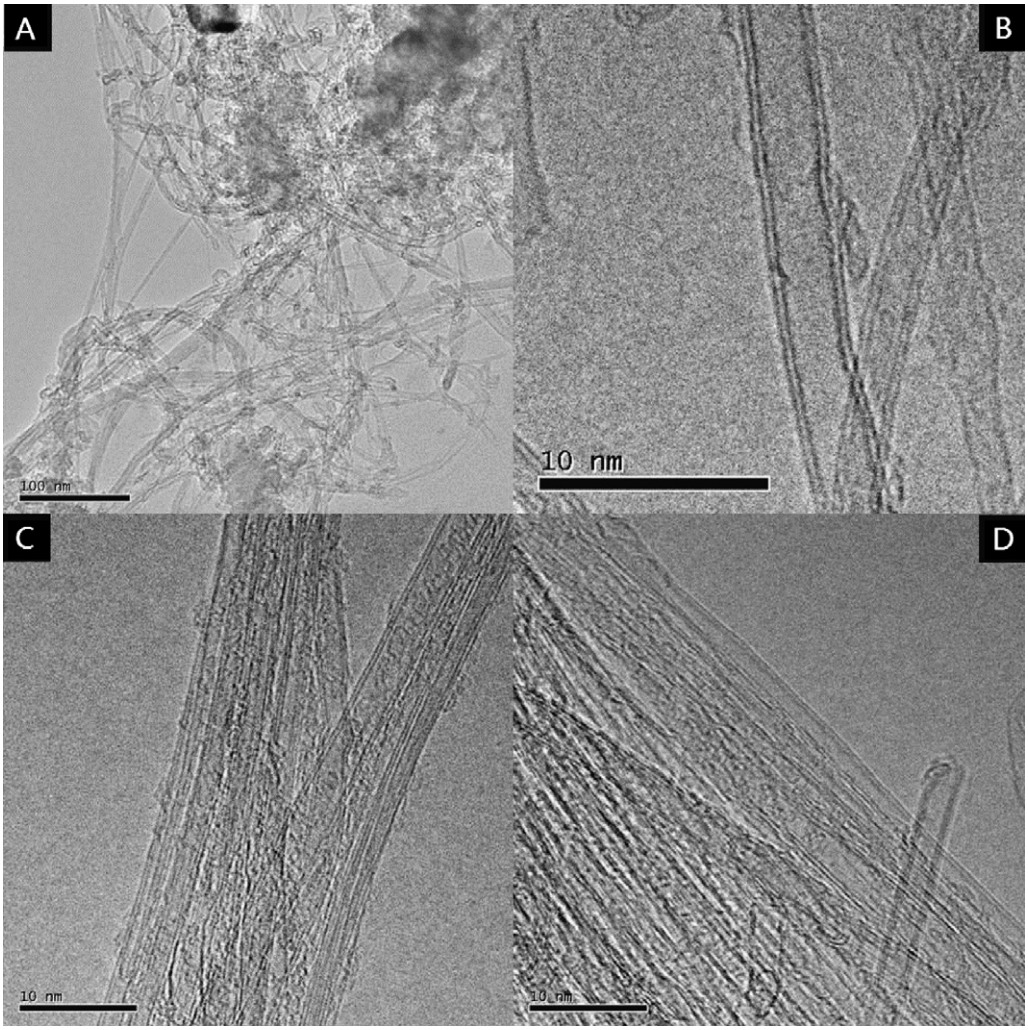

Fig. 5. HRTEM images of DWCNTs produced with different content of water vapor in the feed (A–D) 0 ppm, (E and F) 460 ppm, (G and H) 930 ppm, (I and J) 1400 ppm, (K and L) 1970 ppm.

characterization. Fig. 2 shows the XRD patterns of the MgO support (used as a reference), Co/MgO and Co–Mo/MgO. Compared to the pattern of MgO, Co/MgO has the diffraction peaks with similar positions but with lower intensities. Since CoO and MgO both possess a rock-salt type crystal structure and have the similar ionic radius (0.066 nm for Mg^{2+} and 0.065 nm for Co^{2+}), the diffraction peaks of CoO could be masked by the corresponding peaks of MgO. Additionally, a solid solution may be formed between CoO and MgO [45,48–50]. However, the existence of the peak of Co_3O_4 (as shown in Fig. 2b) indicates that just a portion of Co oxide dissolves into the matrix of MgO. It has been reported that a complete dissolution of CoO in MgO occurs at temperature higher than 800 °C producing $Co_xMg_{1-x}O$ [51]. Thus, it is inferred that after calcination of the Co/MgO catalyst at 450 °C, an appreciable part of non-interacting Co_3O_4 phase still exists. For the Co–Mo/MgO, as presented in Fig. 2c, besides the similar diffraction peaks to those of MgO, a small peak for $MgMoO_4$ phase is found as well, while the $CoMoO_4$ phase cannot be identified By XRD. Radwan et al. [51] reported that the stable $MgMoO_4$ and $CoMoO_4$ are easily generated from the interaction between MoO_3 and MgO or CoO at temperature higher than 400 °C. By using extended X-ray absorption fine structure (EXAFS) and X-ray absorption near-edge spectroscopy (XANES) techniques, Herrera et al. [52] suggested the strong interaction between Mo and Co results in a Co molybdate structure in the Co–Mo/SiO_2 catalyst. Thus, the absence of the peaks for $CoMoO_4$ can be attributed to the small particle size of the highly dispersed $CoMoO_4$ phase which may be below the detection limit of the XRD.

Prior to methane catalytic decomposition reaction, the Co–Mo catalysts were reduced at 550 °C for 1 h. Rodriguez et al. [53] employed an in situ XRD to study the reduction of $CoMoO_4$, and their results showed that the peaks of $CoMoO_3$ and $Co_2Mo_3O_8$ are detected during the reduction at 500 °C. It is also reported that $MgMoO_4$ is partially reduced at 800 °C [54]. H_2-TPR profile of the Co–Mo/MgO catalyst is plotted in Fig. 3. The first reduction peak appearing at 470–690 °C may be attributed to the reduction process of $CoMoO_4$ to $CoMoO_x$ ($x < 4$) and the second peak above 690 °C may be due to the further reduction process of $CoMoO_x$ or $MgMoO_4$. This indicates that the pre-reduction in hydrogen at 550 °C could not result in a complete reduction and the formation of metallic Co. However, the partially reduced phase of $CoMoO_x$ ($x < 4$) is formed during the reduction process. In order to understand the structure change of the catalyst during the reaction, the XRD patterns of the Co–Mo/MgO catalysts after the reaction are presented in Fig. 4. Compared to the pattern before reaction (Fig. 2c), the diffraction peaks of CNTs are found in the catalysts after the reaction with no water or with water vapor of 460 ppm, while $MgMoO_4$ and molybdenum carbide are not found, as shown in Fig. 4a and b. However, in the catalyst with the assistance of 4670 ppm water, no peak for carbon materials is found while the phases for the $MgMoO_4$ and $Co_2Mo_3O_8$ are indentified.

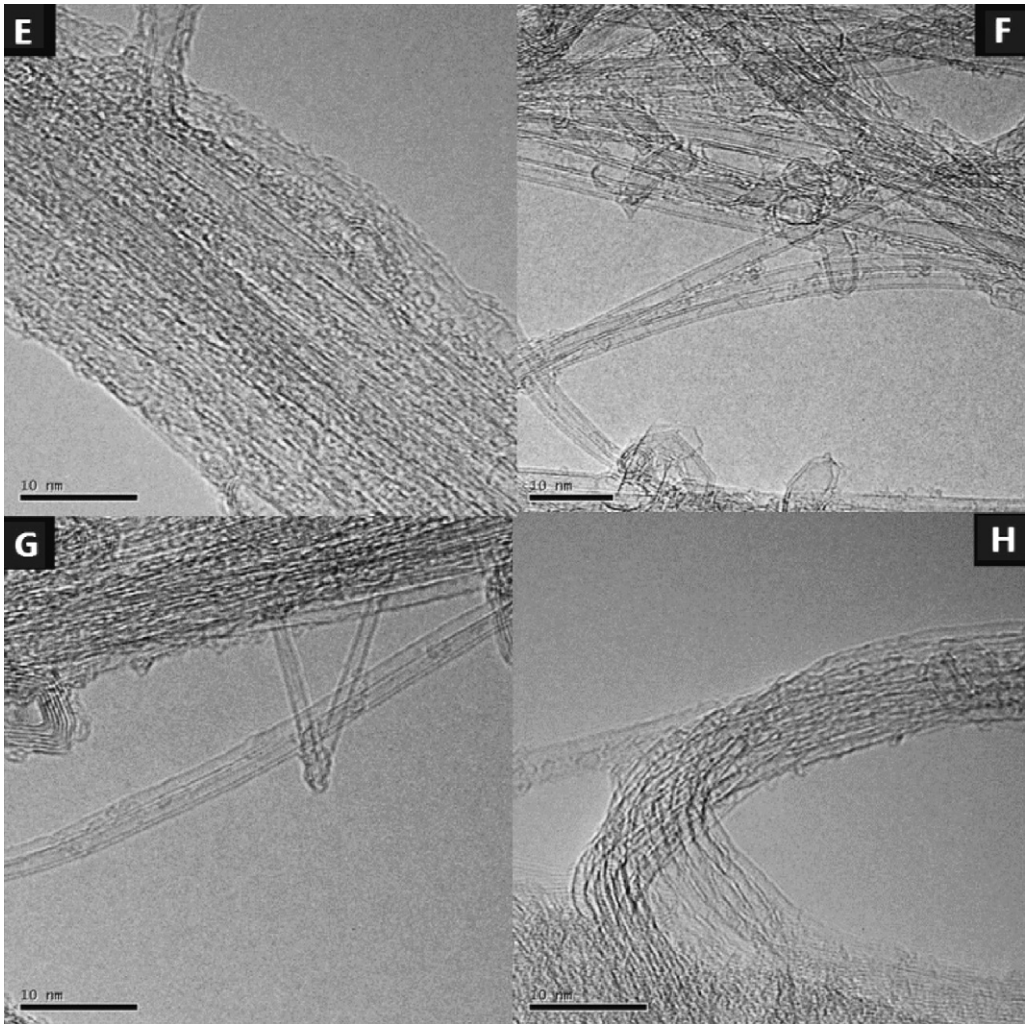

Fig. 5. (*Continued*)

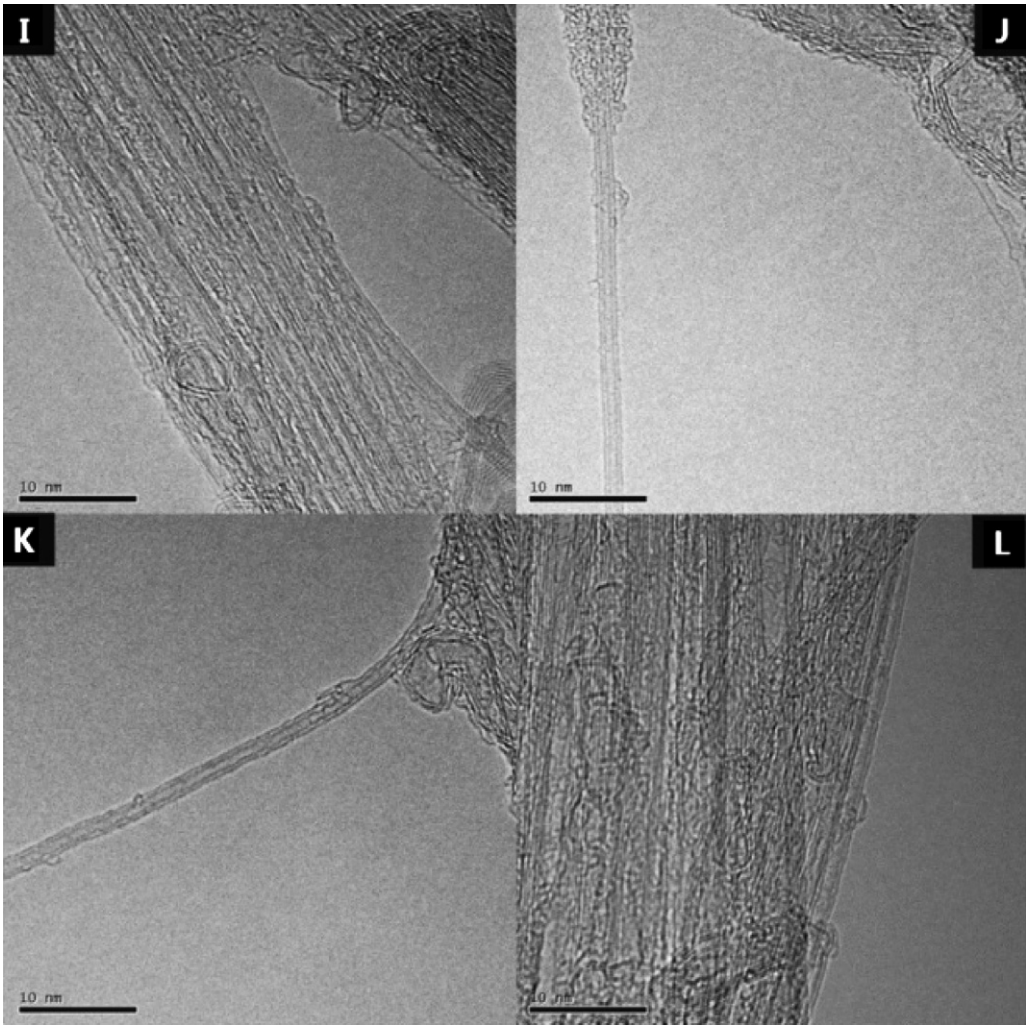

Fig. 5. (*Continued*).

It has been proved that the Mo plays a crucial part for the growth of the SWCNTs in the Co–Mo catalyst. Resasco and co-workers [52,55] used EXAFS and XANES to characterize the state change of Mo during the growth of SWCNTs. Their results showed that oxidized Mo species are transformed into Mo carbide, and this transformation results in releasing the metallic Co in a state of high dispersion, which is responsible for the production of SWCNTs. However, in our case, no Mo_2C is detected with the XRD technique which may be due to the pyrophoricity of Mo_2C in the air during the transfer [56]. The carburization of Mo by methane disrupts the interaction between MgO and MoO_3 or CoO and MoO_3. Released CoO is reduced by methane and the metallic Co acts as the active centre for CNT growth. It is the reason for the disappearing of $MgMoO_4$ phase in the catalyst after methane catalytic decomposition reaction with no water or 460 ppm water. However, when the partial pressure of water is high, the carburization of Mo by methane is depressed. $MgMoO_4$ and $Co_2Mo_3O_8$ become stable, and there is no metallic Co released from the cobalt molybdate which is responsible for the growth of CNTs, thus CNT growth is inhibited.

3.3. Microstructure of solid carbon

HRTEM studies provide direct information on the morphology and microstructure of the prepared CNTs, as shown in Fig. 5. DWCNTs with high purity are obtained under the present conditions. Although some SW, triple-walled (TW) and MWCNTs are also observed by HRTEM, the amount is very low. Fig. 5A–D shows the DWCNTs produced in the reaction without addition of water vapor. Fig. 5A is a low magnification TEM image of the CNTs and Fig. 5B shows an isolated DWCNT with a large diameter clearly, the out diameter and the inner diameter of which are 3.2 and 2.4 nm, respectively. Fig. 5C and D shows the DWCNT bundles. It has been reported that SWCNTs and DWCNTs both have a high tendency to form bundles due to strong van der Waals interaction. Although it is difficult to identify the individual DWCNT in the bundles due to the overlapping of the tubes, the double walls of these tubes are clearly visible on the periphery of the bundles. The diameter distributions of the inner and outer walls for 60 isolated DWCNTs are analysed. The outer diameters and the inner diameters are in the range of 1.6–3.2 and 0.8–2.4 nm, respectively. We observed that the distance between graphene shows the similar interlayer spacing of 0.4 nm, which is consisted with the literature reported [57]. Fig. 5E–L presents the images of the carbon materials formed during the reactions with the addition of water vapor. The DWCNTs with large diameters like the one in Fig. 5B are absence in the DWCNTs produced with the assistance of water which indicates the diameter distribution is narrower than those in Fig. 5A–D. Measurements of 60 individual isolated DWCNTs synthesized with the assistance of 460 ppm water reveals that the outer and the inner diameters of the DWCNTs are in the range of 1.6–2.8 and 0.8–2.0 nm, respectively. When the concentration of water vapor are 930, 1400 and

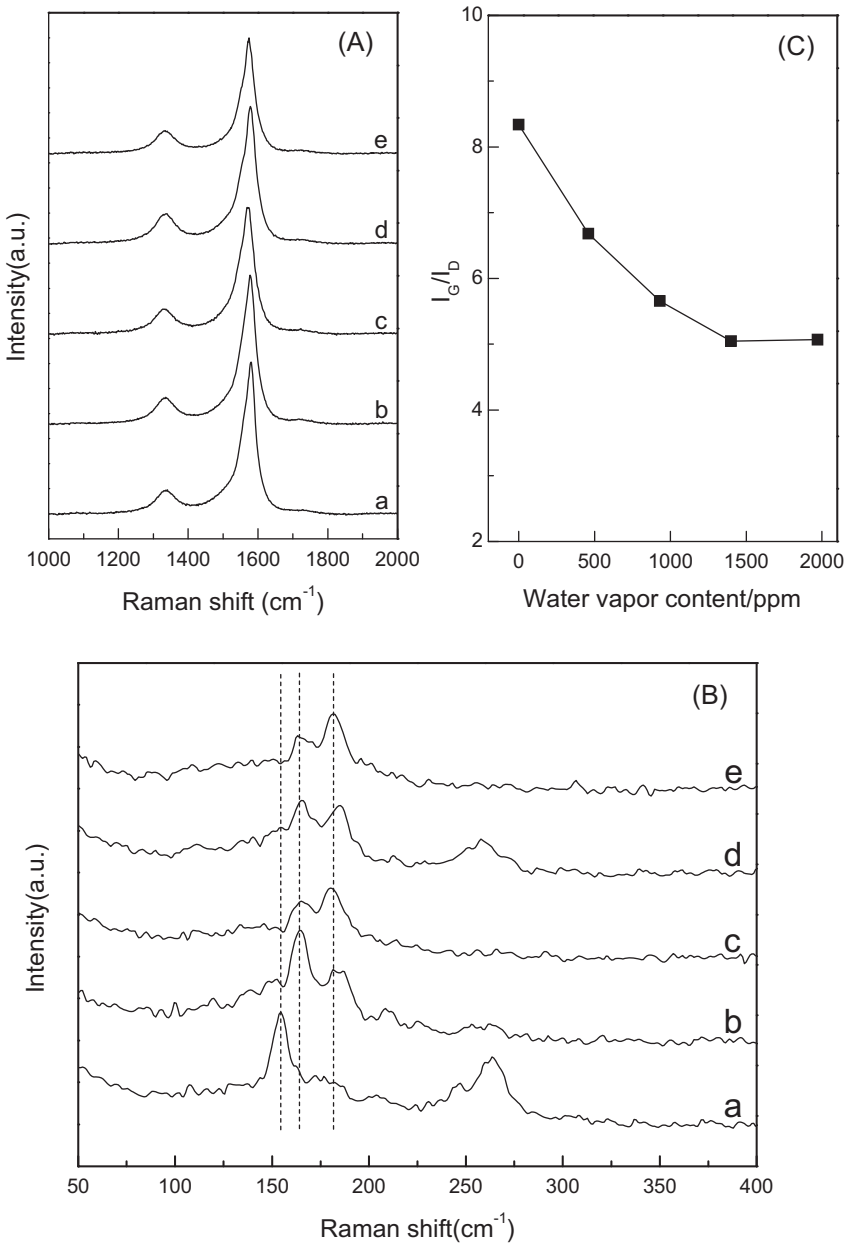

Fig. 6. (A, B) Raman spectra of DWCNTs produced with different content of water vapor: (a) 0 ppm, (b) 460 ppm, (c) 930 ppm, (d) 1400 ppm and (e) 1970 ppm. (C) The relative intensity ratio of the G band (I_G) to D band (I_D) as a function of water vapor concentration.

1970 ppm, no significant change of the DWCNT diameter distribution is observed compared to the DWCNTs produced with the assistance of 460 ppm water vapor.

In addition to HRTEM observation, the Raman spectrum was also employed for the characterization of the DWCNTs. The Raman spectrum (as shown in Fig. 6A) of the DWCNTs excited by a 532 nm wavelength shows a strong G-band intensity at ~1590 cm^{-1}, compared to the D-band intensity at ~1340 cm^{-1}. G-band represents the sp^2 hybrid graphene structure of DWCNTs while the D-band represents the sp^3 hybrid carbon structure which may be amorphous or other disordered carbon structures. The intensity ratio of the G-band to D-bands (I_G/I_D) is calculated, as shown in Fig. 6C. It is interesting to note that the values of I_G/I_D decrease with the increase of water vapor concentration, which reveals the degree of disorder in the synthesized DWCNTs increases with the concentration of water vapor. Water vapor in the feed has been thought as a weak oxidizer which would selectively remove amorphous carbon and maintain the activity of catalyst particles during growth process [26,27]. However, in our experiment not only amorphous carbon is etched by water but also the as-grown DWCNTs are etched by water vapor, which result in the decrease of I_G/I_D. The reason may be attributed to the high concentration water in our case compared with the literatures reported [26,27].

The signals of the radial breathing modes (RBM) which is below 400 cm^{-1} support the existence of DWCNTs or SWCNTs. The position and the presence of the RBM bands depend strongly on the diameter and the chirality of DWCNTs or SWCNTs. The corresponding diameters can be calculated with the equation: $w = 238/d^{0.93}$ [58], where w and d represent the position of the RBM peak and the corresponding diameter, respectively. According to this expression, the diameters of DWCNTs are calculated. The three peaks of the RBM of the DWCNTs produced with no water assistance at 154.5, 247.1 and 263.5 cm^{-1} correspond to the diameter of 1.59, 0.96 and 0.90 nm, respectively, which are ascribed to the inner wall of DWC-

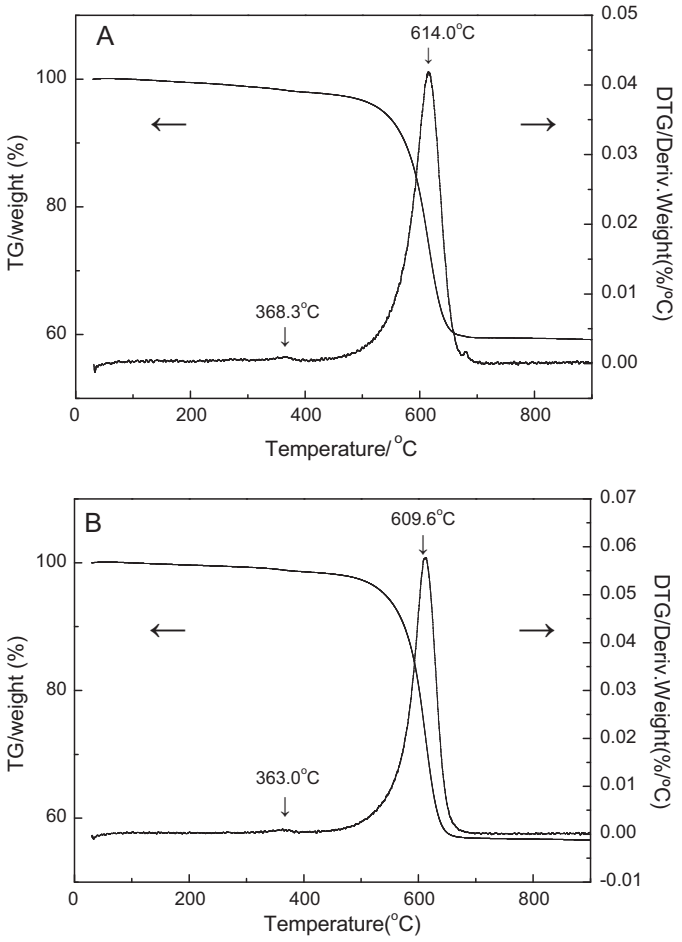

Fig. 7. TG and DTG curves of the as-prepared carbon materials: (A) without water assistance and (B) with 460 ppm water vapor assistance.

NTs since the scattering from outer tubes might not appear [59,60]. The diameters are in the range as that observed from the HRTEM images. It is interesting to note that there is a shift for the RBM signals when the water is introduced into the reaction, as presented in Fig. 6B. The shift to higher position indicates DWCNTs with smaller diameters are produced with the assistance of water, which is consistent with the HRTEM results.

TG and differential thermogravimetric (DTG) curves measured in air of two samples, the one formed without water addition and the other one with 460 ppm water in the feed, are shown in Fig. 7. These curves contain information of the temperature programmed oxidation (TPO) of the carbon samples. According to the literatures [38,61], the amorphous carbon is oxidized at 300–500 °C, the oxidation temperature of DWCNTs is close to 600 °C, while the oxidation temperature of MWCNTs is around 700 °C. There are two peaks in the DTG curve of the sample formed without water vapor (Fig. 7A), locating at 368.3 and 614.0 °C, which are attributed to the oxidation process of amorphous carbon and DWCNTs. The peak centred at 680.0 °C has a low intensity so we ignore it. In the DTG curve of the carbon materials obtained with 460 ppm water addition (Fig. 7B), there are two peaks located at 363.0 and 609.6 °C. From the information of TEM micrograph and Raman spectrum, we were informed that the diameters of the DWCNTs formed with the assistance of water vapour are smaller than those without water. Smaller diameter DWCNTs exhibit a higher reactivity with oxygen due to their greater steric strain [62]. Here, the oxidation temperatures of the smaller diameter DWCNTs produced with water assistance are lower than that of the DWCNTs formed without the assistance of water. Water vapour in the feed may also result in the formation of DWCNTs with more disorder, which also facilitates a lower oxidation temperature. This result is consistent with the Raman characterization, as shown in Fig. 6C.

HRTEM, Raman spectrum and TG characterization results reveal that the addition of small amount of water could reduce the diameter distribution of the DWCNTs. The water in the feed also plays an etching effect on the amorphous carbon and the DWCNTs but cannot eliminate the amorphous carbon completely. DWCNTs produced with the assistance of water may have lots of defects which are beneficial for the functionalization of the outer wall, which is important for the application of DWCNTs.

3.4. Mechanism of water promoting effect

The above mentioned results have shown that a suitable amount of water in the methane feed enhances the initial activity of the catalyst and also increases the yield of DWCNTs, which is consistent with the reported results on SWCNT growth in literatures [26,27,63]. Furthermore, the diameter distribution of the DWCNTs becomes narrower as well if appropriate water is added in the feed. Hu et al. [64] got the similar conclusion about the effect of water vapor on diameter distribution of SWCNTs over a Fe/MgO based catalyst. It has been known that the size of metal particle defines the diameter of the CNTs [65]. The narrow distribution of the DWCNTs indicates that the sizes of the corresponding Co clusters become smaller and the distribution becomes narrow as well. Wen et al. [61] reported that an in situ addition of O_2 is effective in tailoring the diameter distribution of the SWCNTs by tailoring the structure of a Fe–Mo/MgO catalyst. They proposed that the O_2 addition leads to the formation of a Fe–O–Mg species, which inhibits the sintering of Fe clusters and is responsible for the growth of SWCNTs with a narrow diameter distribution. Here, it is likely that a CoO moderated metallic Co phase as Co–CoO formed is via the interaction between water and the metallic surfaces. The Co clusters then exhibit the properties of both metallic Co and oxide CoO on their surfaces, which compose the catalytic sites producing DWCNTs. He et al. [66] proved that the partially reduced Co is effective for the growth of SWCNTs with a narrow diameter distribution. In the water assisted methane decomposition reaction, the oxidative effect of water

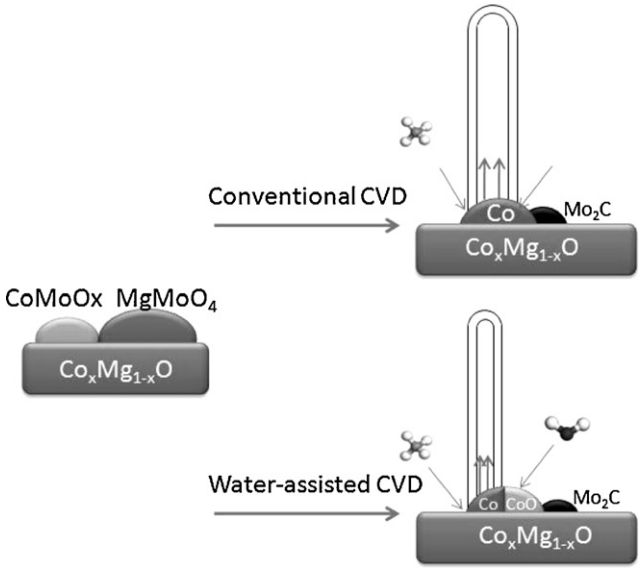

Fig. 8. Schematic of the conventional CVD and water-assisted CVD mechanism.

molecule and the reductive effect of methane may help to maintain the redox cycle of Co/CoO. Partly existing of CoO in the Co clusters decreases the size of the metallic Co and also the strong interaction between Co^{2+} and Co constrains the ripening of the reduced cobalt species, thus provide Co clusters with small and uniform diameters which are responsible for the growth of DWCNTs with small and uniform diameters, as shown in the schematic illustration of Fig. 8.

4. Conclusions

The yield of DWCNTs can be increased and the diameters of the obtained DWCNTs become smaller and uniform if a suitable amount of water is added into the methane feed. When 460 ppm water vapor is added, the yield of DWCNTs can be increased from 47.3 wt.% to 63.4 wt.%. However, no DWCNTs can be produced if 4670 ppm water is added. Too much water inhibits the formation of Co metallic clusters from Co molybdate which are necessary for the DWCNT growth. When an appropriate amount of water vapor is added, a kind of Co–CoO composite clusters may be formed. The sizes of Co metallic clusters decrease due to the formation of CoO in the Co clusters and also the strong interaction between Co^{2+} and Co constrains the ripening of the Co clusters. As a consequence, the growth of thick DWCNTs is suppressed and DWCNTs with small and uniform diameters are synthesized with the assistance of water vapor in the reaction.

Acknowledgements

This work has been supported by the Natural Science Foundation of China under contract number 20736007. The work has been also supported by the Program of Introducing Talents to the University Disciplines under file number B06006, and the Program for Changjiang Scholars and Innovative Research Teams in Universities under file number IRT 0641.

References

[1] S. Iijima, Nature 354 (1991) 56–58.
[2] R.H. Baughman, A.A. Zakhidov, W.A. de Heer, Science 297 (2002) 787–792.
[3] S.S. Fan, M.G. Chapline, N.R. Franklin, T.W. Tombler, A.M. Cassell, H.J. Dai, Science 283 (1999) 512–514.
[4] A.B. Dalton, S. Collins, J. Razal, E. Munoz, V.H. Ebron, B.G. Kim, J.N. Coleman, J.P. Ferraris, R.H. Baughman, J. Mater. Chem. 14 (2004) 1–3.
[5] J.R. Wood, H.D. Wagner, Appl. Phys. Lett. 76 (2000) 2883–2885.
[6] B. Corry, J. Phys. Chem. B 112 (2008) 1427–1434.
[7] W.L. Mi, W.S. Lin, Y.D. Li, J. Membr. Sci. 304 (2007) 1–7.
[8] Y.D. Li, D.X. Li, G.W. Wang, Catal. Today 162 (2011) 1–48.
[9] Y.D. Li, Z.B. Rui, C. Xia, M. Anderson, Y.S. Lin, Catal. Today 148 (2009) 303–309.
[10] Y.D. Li, J.L. Chen, Y.N. Qin, L. Chang, Energy Fuel 14 (2000) 1188–1194.
[11] J.L. Chen, Y.H. Qiao, Y.D. Li, Appl. Catal. A 337 (2008) 148–154.
[12] J.L. Chen, Q. Ma, T.E. Rufford, Y.D. Li, Z.H. Zhu, Appl. Catal. A 362 (2009) 1–7.
[13] J.L. Chen, X. Yang, Y.D. Li, Fuel 89 (2009) 943–948.
[14] Y.D. Li, R. Zhang, J.L. Chen, X.M. Li, Zaragoza Spain, 2nd European Hydrogen Energy, 2005.
[15] X. Li, Z.H. Zhu, J.L. Chen, R.D. Marco, A. Dicks, J. Bradley, G.Q. Lu, J. Power Sources 186 (2009) 1–9.
[16] Q.H. Liu, Y. Tian, C. Xia, L.T. Thompson, B. Liang, Y.D. Li, J. Power Sources 185 (2008) 1022–1029.
[17] L.J. Jia, Y. Tian, Q.H. Liu, C. Xia, J.S. Yu, Z.M. Wang, Y.C. Zhao, Y.D. Li, J. Power Sources 195 (2010) 5581–5586.
[18] M.J. Bronikowski, P.A. Willis, D.T. Colbert, K.A. Smith, R.E. Smalley, J. Vac. Sci. Technol. A 19 (2001) 1800–1805.
[19] S. Iijima, T. Ichihashi, Nature 363 (1993) 6030–6035.
[20] A. Thess, R. Lee, P. Nikolaev, H.J. Dai, P. Petit, J. Robert, C. Xu, Y.H. Lee, S.G. Kim, A.G. Rinzler, D.T. Colbert, G.E. Scuseria, D. Tomanek, J.E. Fischer, R.E. Smalley, Science 273 (1996) 483–487.
[21] J.F. Colomer, C. Stephan, S. Lefrant, G. van Tendeloo, I. Willems, Z. Konya, A. Fonseca, C. Laurent, J.B. Nagy, Chem. Phys. Lett. 317 (2000) 83–89.
[22] A.M. Cassell, J.A. Raymakers, J. Kong, H.J. Dai, J. Phys. Chem. B 103 (1999) 6484–6492.
[23] J. Kong, A.M. Cassell, H.J. Dai, Chem. Phys. Lett. 292 (1998) 567–574.
[24] L.Y. Piao, Y.D. Li, J.L. Chen, L. Chang, J.Y.S. Lin, Catal. Today 74 (2002) 145–155.
[25] A. Cordier, V.G. de Resende, A. Weibel, E.D. Grave, A. Peigney, C. Laurent, J. Phys. Chem. C 114 (2010) 19188–19193.
[26] K. Hata, D.N. Futaba, K. Mizuno, T. Namai, M. Yumura, S. Iijima, Science 306 (2004) 1362–1364.
[27] T. Yamada, A. Maigne, M. Yudasaka, K. Mizuno, D.N. Futaba, M. Yumura, Nano Lett. 8 (2008) 4288–4292.
[28] C.L. Pint, S.T. Pheasant, A.N.G. Parra-Vasquez, C. Horton, Y.Q. Xu, R.H. Hauge, J. Phys. Chem. C 113 (2009) 4125–4133.
[29] S.P. Patole, P.S. Alegaonkar, J.H. Lee, J.B. Yoo, Carbon 46 (2008) 1987–1993.
[30] S.P. Patole, P.S. Alegaonkar, J.H. Lee, J.B. Yoo, EPL 81 (2008) 38002–38011.
[31] R. Pfeiffer, T. Pichler, Y.A. Kim, H. Kuzmany, Carbon Nanotubes 111 (2008) 495–530.
[32] A. Gruneis, M.H. Rummeli, C. Kramberger, A. Barreiro, T. Pichler, R. Pfeiffer, H. Kuzmany, T. Gemming, B. Buchner, Carbon 44 (2006) 3177–3182.
[33] S.C. Lyu, T.J. Lee, C.W. Yang, C.J. Lee, Chem. Commun. 12 (2003) 1404–1405.
[34] E. Flahaut, R. Bacsa, A. Peigney, C. Laurent, Chem. Commun. 12 (2003) 1442–1443.
[35] W.Z. Li, J.G. Wen, M. Sennett, Z.F. Ren, Chem. Phys. Lett. 368 (2003) 299–306.
[36] J. Zhu, M. Yudasaka, S. Iijima, Chem. Phys. Lett. 380 (2003) 496–502.
[37] A. Bachmatiuk, E. Borowiak-Palen, M.H. Rummeli, C. Kramberger, H.W. Hubers, T. Gemming, T. Pichler, R.J. Kalenczuk, Nanotechnology 18 (2007) 275610–275611.
[38] G.Q. Ning, Y. Liu, F. Wei, Q. Wen, G.H. Luo, J. Phys. Chem. C 111 (2007) 1969–1975.
[39] H. Qi, C. Qian, J. Liu, Nano Lett. 7 (2007) 2417–2421.
[40] Y. Liu, W.Z. Qian, Q. Zhang, G.Q. Ning, G.H. Luo, Y. Wang, D.Z. Wang, F. Wei, Chem. Eng. Technol. 32 (2009) 73–79.
[41] M. Zdrazil, Catal. Today 86 (2003) 151–171.
[42] T. Klicpera, M. Zdrazil, J. Catal. 206 (2002) 314–320.
[43] B. Kitiyanan, W.E. Alvarez, J.H. Harwell, D.E. Resasco, Chem. Phys. Lett. 317 (2000) 497–503.
[44] M.H. Hu, Y. Murakami, M. Ogura, S. Maruyama, T. Okubo, J. Catal. 225 (2004) 230–239.
[45] M. Shajahan, Y.H. Mo, A.K.M. Fazle Kibria, M.J. Kim, K.S. Nahm, Carbon 42 (2004) 2245–2253.
[46] B.C. Liu, S.C. Lyu, S.I. Jung, H.K. Kang, C.W. Yang, J.W. Park, C.Y. Park, C.J. Lee, J. Chem. Phys. Lett. 383 (2004) 104–108.
[47] H. Ago, N. Uehara, N. Yoshihara, M. Tsuji, M. Yumura, N. Tomonaga, T. Setoguchi, Carbon 44 (2006) 2912–2918.
[48] A.K.M. Fazle Kibria, M. Shajahan, Y.H. Mo, M.J. Kim, K.S. Nahm, Diamond Relat. Mater. 13 (2004) 1865–1872.
[49] E. Flahaut, A. Peigney, C. Laurent, A. Rousset, J. Mater. Chem. 10 (2000) 249–252.
[50] S. Tang, Z. Zhong, Z. Xiong, L. Sun, L. Liu, J. Lin, Z.X. Shen, K.L. Tan, Chem. Phys. Lett. 350 (2001) 19–26.
[51] N.R.E. Radwan, A.M. Ghozza, G.A. El-Shobaky, Thermochim. Acta 398 (2003) 211–221.
[52] J.E. Herrera, L. Balzano, A. Borgna, W.E. Alvarez, D.E. Resasco, J. Catal. 204 (2001) 129–145.
[53] J.A. Rodriguez, J.Y. Kim, J.C. Hanson, J.L. Brito, Catal. Lett. 82 (2002) 103–109.
[54] J.E. Miller, N.B. Jackson, L. Evans, A.G. Sault, M.M. Gonzales, Catal. Lett. 58 (1999) 147–152.
[55] W.E. Alvarez, B. Kitiyanan, A. Borgna, D.E. Resasco, Carbon 39 (2001) 547–558.
[56] J.A. Schaidle, A.C. Lausche, L.T. Thompson, J. Catal. 272 (2010) 235–245.
[57] B.C. Liu, S.C. Lyu, T.J. Lee, S.K. Choi, S.J. Eum, C.W. Yang, C.Y. Park, C.J. Lee, Chem. Phys. Lett. 373 (2003) 475–479.
[58] R. Poyato, A.L. Vasiliev, N.P. Padture, H. Tanaka, T. Nishimura, Nanotechnology 17 (2006) 1770–1777.
[59] H.C. Choi, S.Y. Kim, W.S. Jang, S.Y. Bae, J. Park, K.L. Kim, K. Kim, Chem. Phys. Lett. 399 (2004) 255–259.
[60] J.Q. Wei, B. Jiang, D.H. Wu, B.Q. Wei, J. Phys. Chem. B 108 (2004) 8844–8847.
[61] Q. Wen, W.Z. Qian, F. Wei, G.Q. Ning, Nanotechnology 18 (2007) 215610–215611.
[62] I.W. Chiang, B.E. Brinson, A.Y. Huang, P.A. Willis, M.J. Bronikowski, J.L. Margrave, R.E. Smalley, R.H. Hauge, J. Phys. Chem. B 105 (2001) 8297–8301.
[63] D.N. Futaba, K. Hata, T. Yamada, K. Mizuno, M. Yumura, S. Iijima, PRL 95 (2005) 056104–56111.
[64] B. Hu, H. Ago, N. Yoshihara, M. Tsuji, J. Phys. Chem. C 114 (2010) 3850–3856.
[65] E. Lamouroux, P. Serp, P. Kalck, Cat. Rev. Sci. Eng. 49 (2007) 341–405.
[66] M. He, A.I. Chernov, P.V. Fedotov, E.D. Obraztsova, E. Rikkinen, Z. Zhu, J. Sainio, H. Jiang, A.G. Nasibulin, E.I. Kauppinen, M. Niemelä, A.O.I. Krause, Chem. Commun. 47 (2011) 1219–1221.